Kovove Mater. 59 2021 401–414
DOI: 10.4149/km_2021_6_401

Influence of shielding gases on porosity during laser welding of AZ31B magnesium alloy

M. Vyskoč

Slovak University of Technology in Bratislava, Faculty of Materials Science and Technology in Trnava, Advanced Technologies Research Institute, J. Bottu 25, 917 24 Trnava

Received 17 September 2021, received in revised form 5 November 2021, accepted 22 November 2021

Abstract

The paper deals with the evaluation of the shielding gases' influence on the porosity of AZ31B magnesium alloy weld joints produced with disk laser. Butt weld joints were produced under different shielding gas types, namely Ar 4.6, He 4.6, Ar + 5 vol.% He, Ar + 30 vol.% He. Light and electron microscopy, computed tomography, microhardness measurements, and tensile testing were used to evaluate weld joint properties. He shielded weld joints were the narrowest ones (1.79 mm). On the other hand, Ar shielded weld joints exhibited the largest weld width (2.11 mm). The choice of shielding gas had a significant influence on the porosity level of welds. The lowest porosity was observed in weld joint produced in Ar 4.6 shielding atmosphere (only 0.05 mm^3), while the highest level of porosity was detected in weld joint produced in pure He 4.6 (0.41 mm^3).

K e y w o r d s: laser welding, AZ31B magnesium alloy, AZ61 filler wire, porosity

1. Introduction

Light metals and their alloys (Mg, Al, and Ti) are important construction materials with a high strength-to-weight ratio. Magnesium and its alloys have the potential to replace steel and aluminium alloys in many industries such as construction or aeronautics [1–5]. Magnesium is approximately 75 % lighter than steel and 34 % lighter than aluminium [6]. Magnesium and its alloys have specific physical and chemical properties that significantly affect the weldability of the material [7].

Welding of magnesium alloys is closely connected mainly with shrinkage of the weld metal, formation of low-melting phases (γ-$Mg_{17}Al_{12}$), low absorption of laser radiation, low melting point, low evaporation temperature 1100 ℃ [8]. A significant problem resulting from the chemical properties of magnesium is the high affinity of magnesium for oxygen and the subsequent formation of oxide inclusions. This problem occurs mainly with the use of Nd:YAG and Yb:YAG lasers, where their wavelengths (1.06 and 1.03 μm) are assumed to be transparent to $Mg(OH)_2$. For this reason, the $Mg(OH)_2$ layer does not melt and subsequently evaporates (melting point 2800 ℃). Therefore, the preparation of welded surfaces before welding is very important [9–11]. These defects cause problems such as porosity, spatter, instability of the weld pool, hot and liquid cracking of the welded joint. Due to the high thermal conductivity of magnesium alloys, it is essential to use a very high power source for their welding, but this can lead to excessive grain coarsening. Low-melting eutectics are formed along grain boundaries, which increase the susceptibility to hot cracking.

Another problem is deformations and residual stresses caused by high thermal conductivity and a high coefficient of thermal expansion [8]. Mg has no allotropic transformation; it occurs only in the HCP (closest hexagonal packed) structure, which results in poor formability at room temperature. However, at higher temperatures (200–300 ℃), the formability of Mg increases significantly [12, 13]. Hot cracking, oxide inclusions, and the formation of brittle intermetallic compounds often occur in conventional fusion welding methods [14].

Laser welding is a fusion process of joining materials, which uses highly concentrated energy to heat

*Corresponding author: e-mail address: maros.vyskoc@stuba.sk

Table 1. Chemical composition and mechanical properties of the base material of AZ31B magnesium alloy and chemical composition of AZ61 filler wire

Chemical composition of AZ31B (wt.%)	Fe	O	N	C	H	Ti
	≤ 0.3	≤ 0.25	≤ 0.03	≤ 0.1	≤ 0.0125	Balance
Mechanical properties of AZ31B	R_m (MPa)	$R_{p0.2}$ (MPa)	A_{50} (%)	HV		
	570	540	21	210		
Chemical composition of AZ61 (wt.%)	Al	Zn	Th	Mn	Cu	Mg
	6.5	1	0.3	0.20	0.03	Balance

and melt basic materials [15, 16]. Laser welding is a promising process of joining materials due to high energy density, narrow weld bead and heat-affected zone, penetration depth, high cooling rate, and consequently the limited formation of intermetallic phases [17–20]. The heat-affected zone in the weld is usually much narrower than with other conventional welding methods. These intermetallic phases form a layer in the interdendritic spaces. The thickness of this layer affects the strength of the welded joint [21–23].

Shielding gases have an important effect on the formation of weld beads and penetration. The application of different shielding gases can result in different penetration and weld bead profiles. The pores can be the starting point for crack propagation in the welded joint and can significantly reduce the life cycle of the joints under dynamic loads. From the above, it is clear that the appropriate choice of process gases is an essential aspect for the efficiency, quality, and overall acceptability of the weld [24]. Argon (Ar) and helium (He) are inert gases that do not affect metallurgical processes during welding [25]. Both are often used to protect the weld pool from the ambient atmosphere, where Ar is usually the preferred choice due to lower costs. The composition of the shielding gas affects not only the heat distribution in the weld but also the shape of the weld and the welding speed. Two-component mixtures of Ar and He are the most satisfactory choice. They work by being associated with minimal defocusing of the incident laser beam. Combinations with not very large amounts of Ar appear to be almost as good as pure helium, not only because they do not significantly increase defocusing but also because they have the additional advantage of minimizing costs [26]. In order to optimize the laser welding process and ensure high weld quality, it is necessary to understand the effect of shielding gas on the overall properties of welded joints. Therefore, the paper deals with the types of shielding gases for the formation of porosity in the weld metal.

In the present study, the AZ31B alloy is investigated, where the main alloying elements are aluminium and zinc. Aluminium increases strength, hardness and improves castability. In addition to increased hardness and strength, zinc also improves toughness. The amount of Zn is limited due to the formation of hot cracks during solidification. The designation B means the class (purity) of the alloy, and H24 expresses the processing of the alloy – strain hardened and partially annealed [27]. The disadvantage of Mg-Al-Zn-(Mn) alloys is their limited possibility of use at higher temperatures because the mechanical properties deteriorate significantly when exposed to temperatures higher than 120 ℃ [28]. These selected properties are similar to aluminium alloys, so the conditions for welding are practically identical. Nevertheless, it is possible to produce laser welds using suitable welding parameters in wrought magnesium alloys without cracks, with low porosity and good quality [9].

2. Experiment

2.1. Material characteristics

As experimental material for this research, AZ31B magnesium alloy was used. The thickness of the base material was 2 mm. Due to the intensive evaporation of alloying elements (Mg and Zn elements), a filler wire with higher alloying AZ61 (6 % Al + 1 % Zn) was used during welding. Butt welds were produced using a disk laser. The chemical composition of the AZ31B base material and its mechanical properties are given in Table 1. Also, the chemical composition of the filler wire AZ61 is given in Table 1.

2.2. Laser equipment and welding parameters

Welds were created in continuous mode using a TruDisk 4002 disk laser with a maximum power of 2 kW. The wavelength of the laser radiation was 1.03 μm, and the beam quality (BPP) was 8 mm mrad^{-1}. The laser beam was led to the BEO D70 focusing optics using an optical cable with a diameter of 400 μm. The size of the beam spot on the surface of the base material was 400 μm. The focal

Table 2. Welding parameters

No.	Power (kW)	Welding speed ($mm\,s^{-1}$)	Type of shielding gas	Shielding gas flow rate ($l\,min^{-1}$)	Focusing (mm)
1	2	40	Ar + 30% He	30	0
2	2	40	Ar + 5% He	30	0
3	2	40	He 4.6	30	0
4	2	40	Ar 4.6	30	0

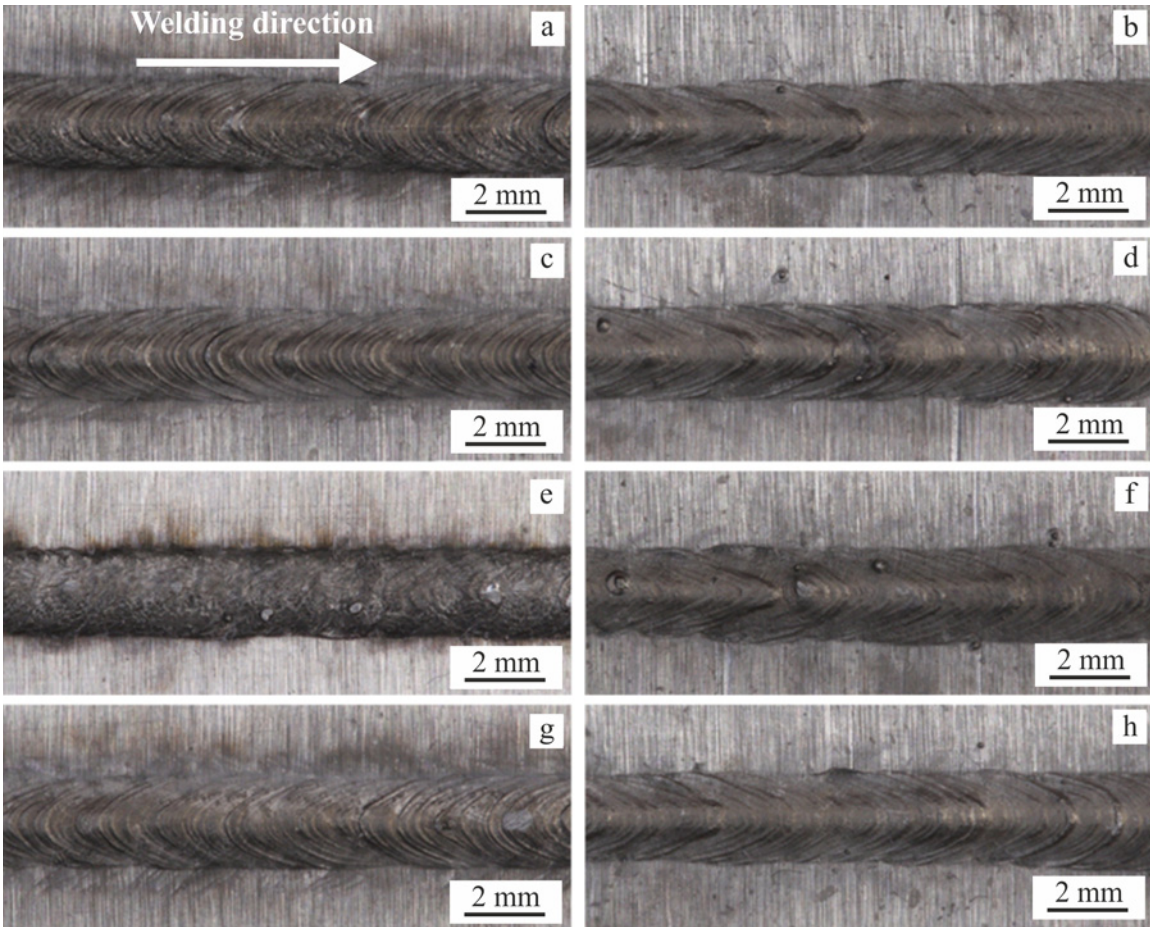

Fig. 1. Weld beads and roots of weld joints: (a), (b) Ar 4.6; (c), (d) Aluline He5; (e), (f) He 4.6; (g), (h) Aluline He30.

length was 200 mm. The focusing optics were mounted on a 6 angular industrial robot Fanuc M-710iC/50. During welding, the surface and root of the weld were protected from the ambient atmosphere. The type of shielding atmosphere changed; the other welding parameters were constant: power 1.9 kW, welding speed $40\,mm\,s^{-1}$, and focusing 0 mm. Welding parameters are given in Table 2.

2.3. Preparation of welded joints

Metallographic sample preparation was performed according to the standard for macroscopic and microscopic analysis of samples STN EN ISO 17639. Weld cross-sections were electrolytically etched in Picral reagent for 8 s (chemical composition: 100 ml ethanol and 4.2 g picric acid). The macrostructure and microstructure of the welded joints were analysed with a NEOPHOT 32 light microscope. For a more detailed analysis of the microstructure, a JEOL 7600 F scanning electron microscope was used. A coordinate measuring instrument based on a Zeiss Metrotom 1500 computed tomography was used to identify the porosity present in the laser welds and its location in the welds. Computed tomography (CT) was able to measure size, distribution, and total porosity volume. After the tensile test, the fracture surfaces were analysed by SEM. The microhardness was measured according

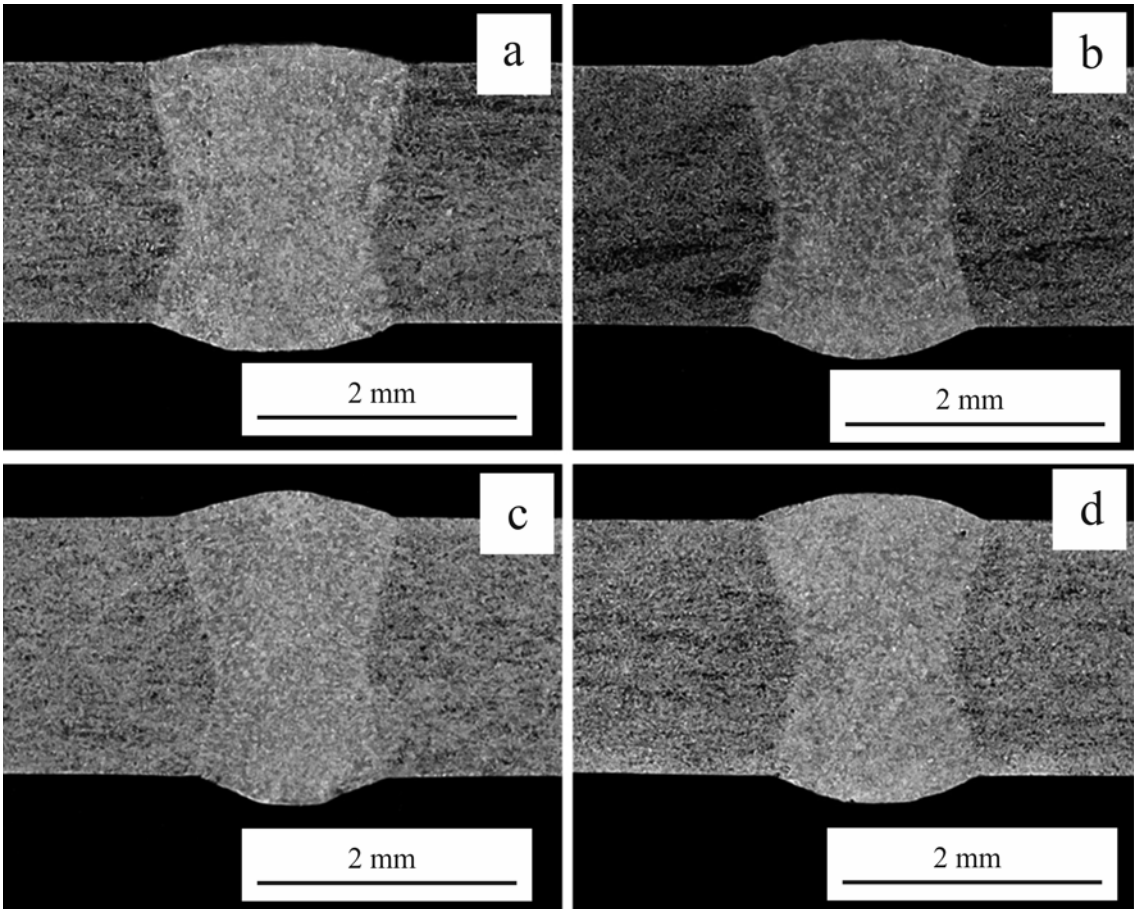

Fig. 2. Cross-sections of weld joints produced under different shielding gases: (a) Aluline He, (b) Aluline He30, (c) He 4.6, and (d) Ar 4.6.

to Vickers on an IndentaMet 1100. The measurement parameters were as follows: load 100 g with a load time of 10 s. The distance between the indents in WM was 200 μm and in HAZ 300 μm. The static tensile test was performed at room temperature on a Tinius Olsen 300 ST shredder (max. load force 300 kN) at a speed of 5 mm s^{-1}.

3. Results

3.1. Surfaces and roots of welded joints

The weld bead and roots of the joints of the AZ31B magnesium alloy are shown in Figs. 1a–h. The welding direction is indicated by an arrow. Figures 1a,b show the weld bead and root of a welded joint produced at a laser beam power of 1.9 kW, a welding speed of 40 mm s^{-1}, a focus of 0 mm, and the protection of the melting pool with Ar 4.6. The weld bead has a regular shape without the presence of a spatter. The root of the weld also has a regular shape. Another weld of Figs. 1c,d was created at the same welding parameters as in the previous case, but Ar + 5 % He (Aluline He5) was used to protect the weld metal. It is evident that the width of the welded joint is smaller than in the previous case. The root of the weld has a regular shape. A slight spatter of weld metal in the root area was recorded. Figures 1e,f document the joint produced at shielding gas of He 4.6. The weld bead of the weld joint and the root exhibit a regular width. The presence of oxidation is visible on the surface, which was caused by insufficient gas protection of the melting pool from the ambient atmosphere. It was at this weld that the narrowest joint width was measured. When using Ar + 30 vol. % He (Aluline He30) for weld metal protection (Figs. 1g,h), the average weld width was larger compared to previous cases. The weld bead exhibits a regular shape. The root of the weld joint exhibits a regular shape without the presence of a spatter.

Cross-sections of welded joints created by using different types of shielding gases are shown in Fig. 2. The welded joint in Fig. 2a was produced using Ar 4.6. The width of the weld bead is 2.11 mm, and the root width is 1.91 mm. The weld joint has slight excess weld metal (0.15 mm), and its root is excessively penetrated (0.21 mm). The surface of the weld bead (Fig. 2b) produced under Aluline He5 has excess metal

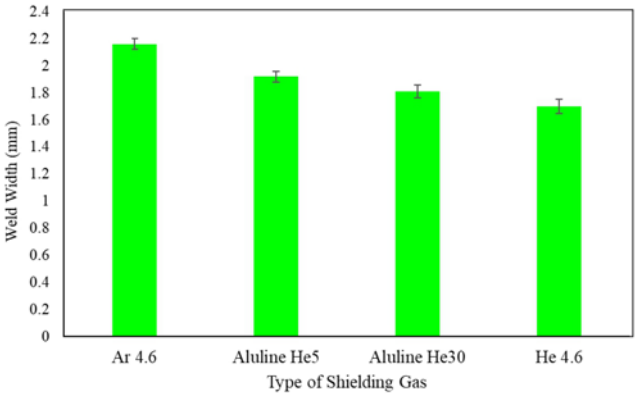

Fig. 3. Influence of type of shielding gas on weld width.

(0.21 mm). The reason for excess metal on the surface base material is the use of filler wire. Its root is excessively penetrated (0.24 mm). The width of the weld bead is 1.95 mm, and the width of the weld root is 1.82 mm. The surface of the weld bead (Fig. 2c) created under He 4.6 also has excess metal (0.2 mm), and its root is excessively penetrated (0.23 mm). The width of the weld bead dropped to 1.79 mm and the root width to 1.47 mm. When using the shielding gas Aluline He30 (Fig. 2d), there was no significant change compared to the previous case. The measured excess metal was 0.22 mm, and the root was excessively penetrated (0.21 mm). The measured width of the weld surface was 1.83 mm and its root 1.62 mm. In terms of geometry, there was no significant influence by using the different types of shielding gases on the geometry of individual welded joints.

The influence of shielding gases on the width of the welded joint is shown in Fig. 3. Widths were measured at three locations on each weld. As the results show, the narrowest weld joint was produced under He 4.6 as the shielding atmosphere (1.79 mm). In contrast, the widest weld was recorded using shielding gas Ar 4.6 (2.11 mm). The addition of helium to obtain a gas mixture of Aluline He5 and Aluline He30 did not result in a significant change in the widths of the weld beads compared to pure He 4.6 and Ar 4.6. In arc welding, the voltage on the arc increases with increasing He content. This is attributed to the higher ionization potential of helium compared to argon. This means that more heat is transferred to the base material. This creates a larger molten area [29]. A different situation was observed during laser welding. The helium-protected joints were smaller in width compared to the welds created under Ar and its mixtures. This fact is attributed to the higher ionization potential of helium and thus to the smaller formation of the laser-induced plasma. In this case, the laser beam is not defocused by the plasma above the material's surface as in the use of Ar. The energy density is higher, i.e., the laser beam is concentrated to a small spot, resulting in a narrow, deep penetrated weld joint. In addition, the low molecular weight of helium increases the recombination between metal ions and plasma electrons, creating a less dense plasma cloud. In contrast, argon is ionized relatively easily because it has a low ionization energy (15.8 eV) and is more prone to plasma formation. The plasma generated above the metal surface causes the incident laser beam to defocus. The energy density decreases, the weld becomes shallower. These results are consistent with a study by Katayama et al. [30], who examined the effect of the defocused distance on the penetration depth of a laser weld. They found that the plasma He is formed by the emission of neutral metal atoms emanating from the steam-gas channel during welding, while in Ar or N2, it is formed under the nozzle next to the keyhole. Ahn et al. [31] found that the width of the weld joint created by using argon was wider than that of the weld joint produced in a helium shielding atmosphere. The same result was found when comparing the root widths of welds. In contrast, the weld was wider when He was used as a shielding gas at 4 and 5 m/min welding speeds. The authors explained this by the fact that higher ionization potential and higher thermal conductivity He increased the thermal energy introduced into the material. Reisgen et al. [32] found that weld joints were shallow when Ar was used as the shielding atmosphere. They explained that this was due to a plume formation above the weld metal and thus instability of the welding process, which caused spatter and a poor surface appearance of the weld joint.

3.2. Light and electron microscopy

Figures 4a–f show the microstructures of AZ31B magnesium alloy welded joints fabricated under different shielding gases. The microstructure of the base material is shown in Fig. 4a. It is clear from the figure that the microstructure has a polyhedral character with a slight heterogeneity in grain size with an average size of 21.8 µm. Figure 4b shows a transition area from BM to WM. Grain refinement has occurred in the weld metal, and the microstructure is formed by fine dendrites. Figure 4c shows a welded joint created under Ar 4.6. The heat-affected zone is indistinct. The weld metal microstructure has a dendritic morphology with very fine dendrites. It can be assumed that the dendrites are formed by a solid solution of Al in Mg, and γ-phase ($Mg_{17}Al_{12}$) and β-phase (Mg_2Al_3) are precipitated in the interdendritic space. In his study, Hadzima [33] found that the microstructure of the base material consists of a solid solution of δ, which is the primary base solid solution of aluminium in magnesium and has a hexagonal crystal structure $\gamma + \delta$ eutectic and AlMn-based particles. At the grain boundaries, the intermetallic phase γ with

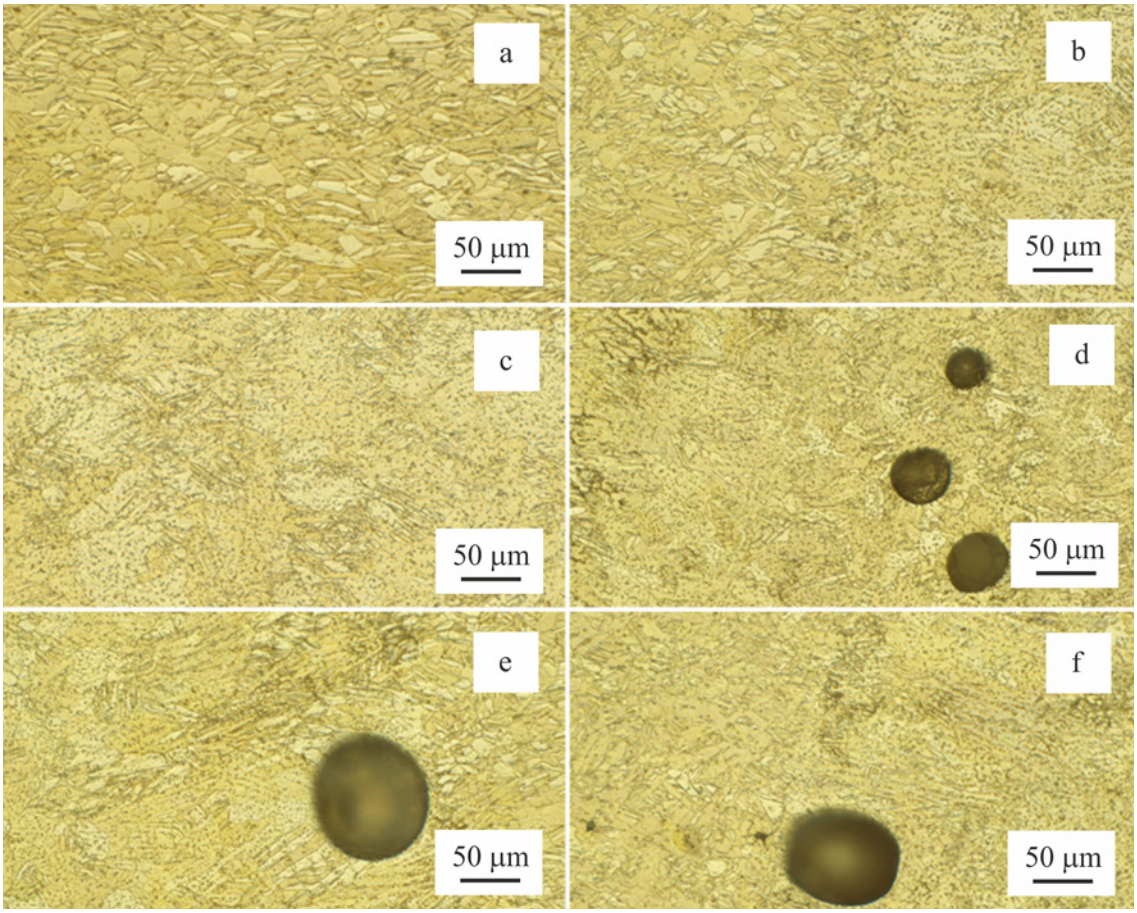

Fig. 4. Microstructures of welds: (a) BM, (b) BM-HAZ, (c) Ar 4.6, (d) Aluline He30, (e) He 4.6, and (f) Aluline He5.

the composition $Mg_{17}Al_{12}$, which has a cubic structure and is in the form of a discontinuous precipitate, precipitates during solidification. Phase R represents the compound $Al_{30}Mg_{23}$ (rhombohedral structure), phase β has the composition Mg_2Al_3 (fcc structure), and finally, the solid solution α is a solid solution of magnesium in aluminium with fcc structure. Due to the small amount of alloying elements and poor reactivity with the etchant, it is difficult to observe the structure with a light microscope. In the next weld in Fig. 4d, which was created under Aluline He30, pores trapped in WM can be observed. The largest of them had a diameter of 42 µm. The captured pores probably did not have sufficient time to escape from the melting pool due to the rapid solidification of the weld metal. In their study, Sahul et al. [34] investigated the effect of the surface layer on the properties of welds on magnesium alloy AZ31B. They found that removing the $Mg(OH)_2$ surface layer led to a reduction in the porosity in the weld metal. As in the previous case, the microstructure is formed by very fine dendrites, while the base material is formed by a polyhedral structure. Katayama et al. [12] welded AZ31B magnesium alloy using a disk laser, achieving the same microstructure in the weld metal with the presence of intermetallic phases γ and β in the interdendritic space. Figure 4e shows the microstructure of the WM-BM interface fabricated under shielding gas of He 4.6. Dhahri et al. [35] investigated magnesium alloys AZ91 and WE 43 using a 5 kW CO2 laser, and it has been shown that a shielding gas flow rate of helium less than 50 l min^{-1} can cause spattering and collapse of a keyhole, resulting in the formation of pores in the weld metal. In our case, porosity was also recorded. The pore diameter captured in WM in Fig. 4e represents a value of 104.2 µm. Nakata et al. [36] investigated porosity in magnesium alloys AE42 and AE41. They found that the main element in the gas bubbles in the weld metal was N_2. Hydrogen and argon were present in small amounts. The microstructure of the weld metal (He 4.6) again shows a fine dendritic morphology. Weld (Fig. 4f), which was created under Aluline He5, has an indistinct heat-affected zone. The microstructure is formed of fine dendrites. A pore with a diameter of 96.1 µm was also trapped in the weld metal. Researchers Salleh et al. [37] compared the effect of argon and nitrogen on the porosity in the weld metal. When N_2 was used, no porosity was present in the weld metal. It can be assumed that the γ and β phases are precipitated in the interdendritic spaces. The same results were obtained by Li et

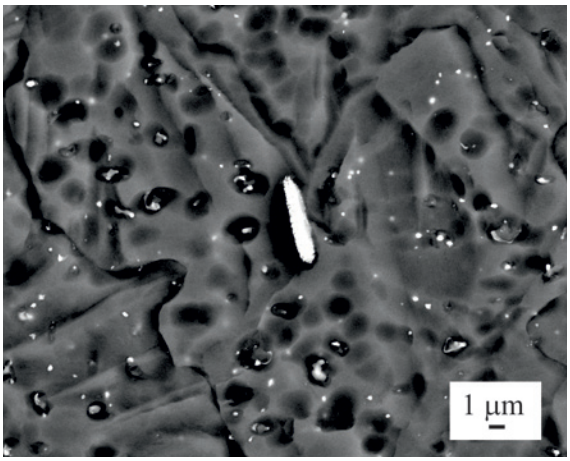

Fig. 5. Microstructure of weld joint produced under Ar 4.6.

al. [38] when the presence of IMC $\gamma(Mg_{17}Al_{12})$ and $\beta(Mg_2Al_3)$ was detected in WM by TEM. The porosity observed in welded joints was probably due to insufficient shielding gas flow rate, which did not provide sufficient protection of the molten metal from the ambient atmosphere, and moisture could enter the pool and cause gas bubbles in the weld metal. The second reason is that the gases trapped in the weld metal did not have enough time to escape from the weld metal to the surface due to its rapid solidification. Haronni et al. [39] found that porosity in the weld metal could be reduced by preheating. A layer of $Mg(OH)_2$ is present on the material's surface, which decomposes to MgO and H_2O when preheated to 300 ℃. Evaporation of H_2O through the steam-gas channel significantly reduced the porosity in the weld metal.

Using an electron microscope, the grain boundaries are already better visible due to the precipitated γ-$Mg_{17}Al_{12}$ intermetallic phase. $Mg_{17}(Al, Zn)_{12}$ phase particles and Al_8Mn_5 particles occur in the alloy. They occur along grain boundaries but also inside grains. Figure 5 documents the weld metal of a welded joint produced under Ar 4.6, which has a dendritic morphology, whereby γ-phase ($Mg_{17}Al_{12}$) and β-phase (Mg_2Al_3) are probably precipitated in the interdendritic spaces. The brighter areas in the weld metal showed the presence of elements with a higher atomic number. TEM would be appropriate to identify intermetallic phases accurately.

3.3. Computed tomography

Some researchers studied the volume of porosity and pore diameter for the mechanical properties of welded joints. Wu et al. [40] observed in their study that the maximum diameter and volume fraction of hydrogen pores ranged from 150 to 280 µm and from 0.35 to 0.75 %. Chen et al. [41] investigated the influence of porosity morphology on mechanical properties. They found that at a laser beam power of 2.8 kW, the porosity volume was 2.78 %, while at a lower laser beam power of 2.3 kW, the porosity volume was 1.83 %. The pore diameter at the higher power of the laser beam was 107 µm, at the lower power 67.3 µm. Another study by Wu et al. [42] observed in laser GMAW hybrid AA7020 welds that most micropores larger than 30 µm in effective diameter had sphericity of approximately 0.60. The authors found only a minimal number of micropores in the upper region of the hybrid weld. On the contrary, the lower region had most micropores smaller than 25 µm in diameter. Fahlström et al. [43] studied the effect of laser welding parameters on porosity of welds in magnesium alloy AM50. The lowest porosity volume of 3 % was achieved for 4 m min^{-1} with 2200 W and two-pass welding at 3 m min^{-1} with 2200 W.

Figures 6a–d show 3D renderings of welded joints produced by using different types of shielding gases. The welded joint fabricated under Ar 4.6 is shown in Fig. 6a. The largest pore had a diameter of 0.57 mm and a pore volume of 0.05 mm^3. The welded joint produced under Aluline He30 is shown in Fig. 6b. The largest pore had a diameter of 0.92 mm, the porosity volume in WM was 0.23 mm^3. In another Fig. 6c, a weld was created under He 4.6. The porosity volume was 0.41 mm^3, and the largest pore diameter was 0.77 mm. The welded joint, the weld metal of which was protected by Aluline He5, is shown in Fig. 6d. The largest pore diameter was 0.63 mm, and the porosity volume was 0.20 mm^3. Pores with a diameter below 50 µm are referred to as micropores. Micropores are associated with hydrogen and other common gases in the case of unsuitable preparation of weld surfaces. Macropores larger than 300 µm significantly affect mechanical properties and are generally located along the central axis of the weld. The keyhole can be the cause of their forming during welding [11]. A possible reason for the formation of pores in the WM is the instability of the steam-gas channel during the welding process. Elements with a low melting point, in our case Mg, evaporate during laser welding and are trapped in the WM, promoting porosity formation [44]. According to Kuo et al. [45], Al_2O_3 is hygroscopic and absorbs ambient moisture. Toda et al. [46] found that the mechanical properties of aluminium alloys are sensitive to the presence of micropores. In addition, they noted that lower ductility, poorer mechanical properties, and fatigue characteristics could be attributed to high-density micropores. They also noted that the tensile strength decreased significantly as the volume of micropores increased.

The sphericity (ψ) of the pores was also calculated according to the formula:

$$\psi = \frac{A_S}{A_P} = \frac{\pi^{\frac{1}{3}} (6V_P)^{\frac{2}{3}}}{A_P}. \quad (1)$$

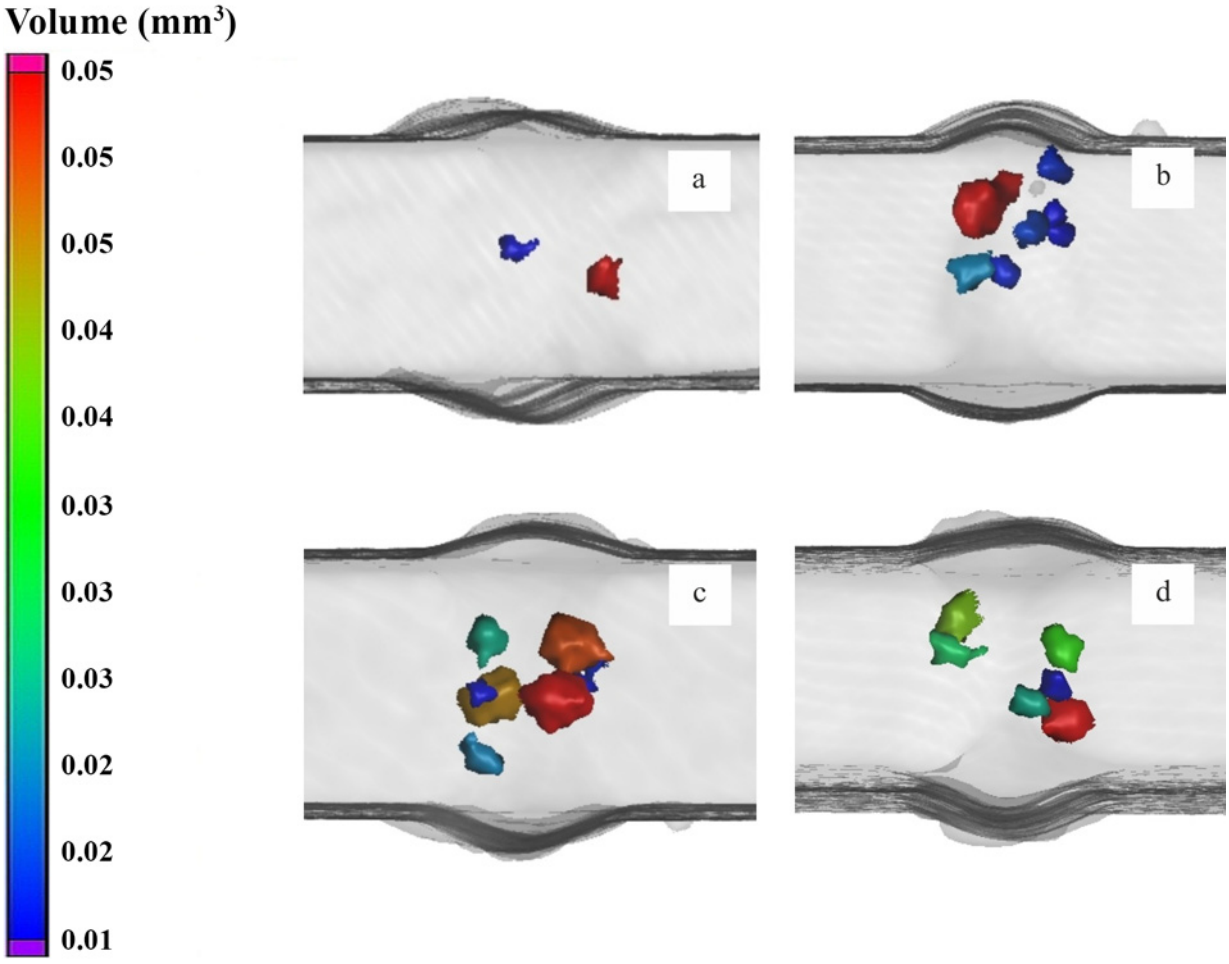

Fig. 6. Porosity results from computed tomography: (a) Ar 4.6, (b) Aluline He30, (c) He 4.6, and (d) Aluline He5.

Table 3. Results from computed tomography under shielding gas Ar 4.6

Radius (mm)	Diameter (mm)	Volume (mm^3)	Surface (mm^2)	Sphericity
0.28	0.57	0.03	0.82	0.57
0.22	0.45	0.02	0.55	0.65

The sphericity of the pores is given by the ratio of the area to the surface of the sphere (with a volume equal to the volume of the pores) of the pore, where A_S and A_P refer to the surface area of the sphere and the pore and V_P is the pore volume. Sphericity measures the shape deviation from the perfect spherical ($\psi = 1$) and measures the extent of deformation for a given pore. The smaller the sphericity value, the more irregular the shape of the pores [47].

The calculated spherical values of ψ pores present in the weld metal at various shielding gases are given in Tables 3–6.

The smallest porosity volume was recorded when the fusion zone of the welded joint was shielded by Ar 4.6. The porosity volume in WM was 0.05 mm^3. The values obtained from computed tomography are given in Table 3.

Another of the studied gases was Aluline He30. A higher porosity volume was recorded for this gas compared to the previous case, namely 0.23 mm^3. The values from computed tomography are given in Table 4.

The use of He 4.6 slightly increased the porosity volume compared to mixed shielding gases. The total volume was 0.41 mm^3. The values from CT are given in Table 5.

As the amount of helium in the mixed shielding gases decreased, the porosity decreased, and therefore it was assumed that at the use of Aluline He5 would be

Table 4. Results from computed tomography under shielding gas Aluline He30

Radius (mm)	Diameter (mm)	Volume (mm^3)	Surface (mm^2)	Sphericity
0.46	0.92	0.12	1.91	0.62
0.25	0.50	0.02	0.60	0.59
0.21	0.42	0.02	0.49	0.73
0.20	0.40	0.01	0.44	0.51
0.22	0.45	0.02	0.52	0.69
0.31	0.63	0.03	0.90	0.52
0.19	0.39	0.01	0.38	0.59

Table 5. Results from computed tomography under shielding gas He 4.6

Radius (mm)	Diameter (mm)	Volume (mm^3)	Surface (mm^2)	Sphericity
0.39	0.77	0.11	1.67	0.66
0.35	0.70	0.09	1.53	0.63
0.39	0.77	0.10	1.61	0.65
0.32	0.63	0.04	0.90	0.63
0.20	0.40	0.01	0.46	0.49
0.22	0.44	0.01	0.44	0.51
0.22	0.44	0.02	0.52	0.69
0.37	0.74	0.03	0.79	0.59

Table 6. Results from computed tomography under shielding gas Aluline He5

Radius (mm)	Diameter (mm)	Volume (mm^3)	Surface (mm^2)	Sphericity
0.30	0.60	0.05	1.04	0.63
0.27	0.54	0.04	0.77	0.73
0.29	0.58	0.04	0.93	0.61
0.31	0.63	0.03	0.82	0.57
0.21	0.42	0.01	0.46	0.49
0.25	0.50	0.03	0.66	0.70

porosity volume lower than that of Aluline He30. The porosity volume was 0.20 mm^3. The values obtained from CT are given in Table 6.

Research has shown that the porosity formation in the weld metal has been reduced when Ar + He mixtures have been used as a shielding atmosphere instead of pure He shielding gas. Similar results were obtained by Takahashi et al. [48], who reported that with Ar shielding gas, the number of pores increased when the laser beam was focused above the sample surface, while with using helium shielding gas, the porosity increased when the beam was focused at the material surface. Panwisawas et al. [49] investigated the influence of welding speed and material thickness on the porosity. They found that the porosity increased with the increase of the material thickness. Also, lower welding speed led to a higher volume of porosity level. There are two types of porosity in the weld metal. In general, process-induced pores have an irregular shape with a relatively larger size compared to metallurgical porosity. Process porosity or cavities are usually induced by the instability of the keyhole during penetration welding. However, for hydrogen gas-induced metallurgical porosity, smaller diameters in the range of 10 to 100 μm can be found [50–53]. If the protection of the weld pool is sufficiently effective, the hydrogen in the weld metal comes mainly from the surface layer of the oxide. Glowacki [54] found that the best combinations range from 0 % Ar and 100 % He to 50 % Ar and 50 % He (per unit volume of gas mixture). Gaseous mixtures of Ar + He with less than 50 % He lead to a significant defocusing of the incoming laser beam by the plasma cloud above the laser-generated keyhole. The plasma formation is crucial to the welding operation. However, this is not a serious problem for welded joints created with a disk laser due to the shorter wavelength of the laser beam, namely 1.03 μm. The emitted radiation is less absorbed by the plasma above the surface of the welded material. However, Gao et al. [55] found when the laser power was in their study lower than 5 kW, the laser power absorbed by the plume was no more than 5 % because it was

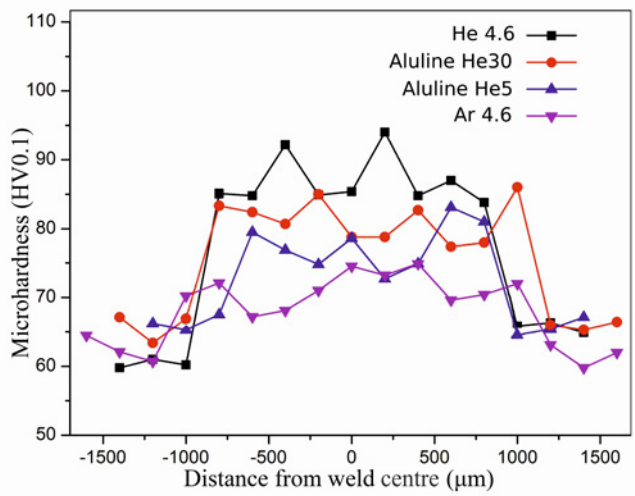

Fig. 7. The course of microhardness using different types of shielding gases.

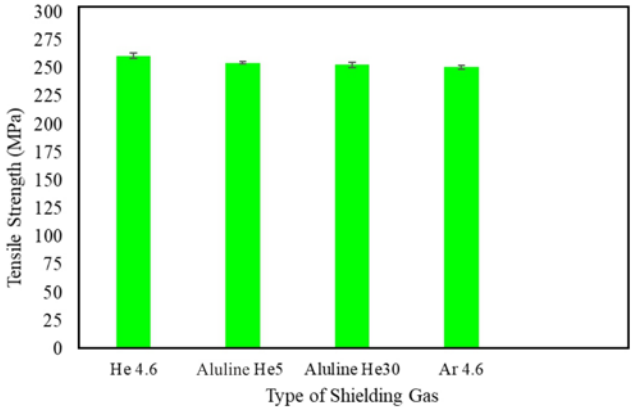

Fig. 8. Effect of shielding gases on the strength of weld joints.

a weakly ionized plasma. At that stage, the plasma shielding effect could be ignored, and the weld penetration depth increased with laser power proportionally. However, when the laser power was higher than 5 kW, the laser power absorbed by the laser plume was up to 24 %. Only larger pores were found within the CT.

Further research must be aimed with the computer microtomography, i.e., utilization of reducing pixel size. Slotwinski et al. [56] found that some samples had pores that were not measurable by X-ray CT, which can be seen using a pixel size of 2.4 µm. There, the pores could be several times smaller than those seen in X-ray CT scans. Detection of smaller pores by µCT may be associated with the influence of segmentation algorithms on the detected porosity. Heim et al. [57] found that "Isodata" primarily detects small pores, while "0.0" detects the largest pores. "Isodata" has been found to be the strongest algorithm that detects most pores in terms of volume and number of pores.

3.4. Microhardness of weld joints

The course of microhardness of weld joints produced by using different types of shielding gases is shown in Fig. 7. As can be seen from the figure, the microhardness of the weld metal is higher at all joints compared to the base material. This increase in microhardness is associated with a lower heat input, which is characteristic of laser beam welding and alloying the weld metal using AZ61 filler wire. As can be seen from the measured microhardness values, the effect of the shielding gases used in the welding was obvious. Using Ar 4.6 shielding gas, the smallest average microhardness of the weld metal was measured, namely 71.2 HV0.1 (± 0.6). Using an Ar gas mixture with 5 % He, the average microhardness increased to 78.9 HV0.1 (± 1.0). When Aluline He 30 (70 % Ar + 30 % He) was used, the average microhardness increased to 82.2 HV0.1 (± 0.6) compared to the previous case. The average microhardness of the weld metal 87.9 HV0.1 (± 0.5) was recorded under He 4.6 shielding gas, which was also the highest average microhardness. Dhahri et al. [58], in their study, welded the WE43 magnesium alloy using a 5 kW CO2 laser. They found that helium proved to be the best depending on the drawing of the weld bead, the penetration, and the depth/width ratio of the welded joint. At the same time, they noted that the shielding gas flow rate should not be less than 50 l min^{-1}, which can cause spatter or collapse of the keyhole. In another study, researchers focused on comparing He and Ar shielding gases in laser welding of magnesium alloys. They found that He shielding gas has a better protective effect on the weld pool in welding magnesium alloys than Ar due to its higher ionization potential and better conductivity [35].

3.5. Tensile test

The dependence of the tensile strength on the type of shielding gas is shown in Fig. 8. The highest tensile strength of 261 MPa (± 2.4) was recorded when He 4.6 shielding gas was used. A lower tensile strength of 255 MPa (± 1.8) was recorded for Aluline He5. Using Ar 4.6 shielding gas, an average tensile strength of 253 MPa (± 1.3) was measured. A lower value of 251 MPa (± 1.3) was found when Aluline He30 was used. The presence of porosity in the weld is one of the main problems in the laser welding of magnesium alloys. The high porosity content is one of the most important factors that cause the low strength of welded joints, although their size is smaller than the grain size of the base material [59]. In a tensile test, due to the concentration of stress around the pores, microcracks

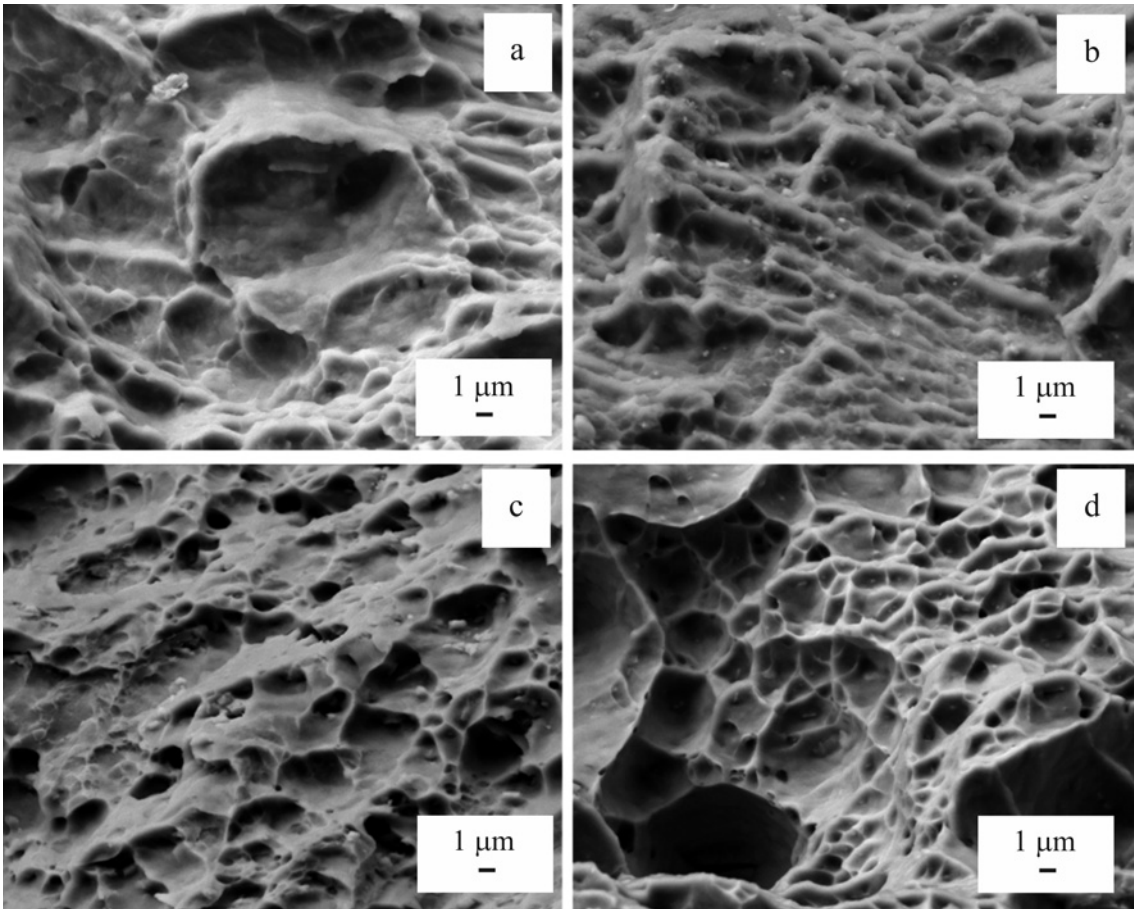

Fig. 9. (a)–(d) fracture surfaces ductile fractures.

are usually initiated, and therefore a fracture occurs in the weld metal [60]. Magnesium has a significantly high hydrogen solubility in the liquid phase, and the porosity of magnesium alloys depends on the amount of dissolved hydrogen [61]. The permissible hydrogen content in welds can depend on many factors, such as the welding process parameters, the chemical composition of the alloys, the solidification time, the thermal gradient, the structure of the weld, and the concentration of inclusions. In zirconium-containing magnesium alloys, hydrogen will react with the zirconium to form ZrH_2, and finally, in this case, the porosity of the hydrogen will not be a problem [62, 63].

3.6. Analysis of fracture surfaces

The results of the analysis of the fracture surfaces are shown in Figs. 9a–d. An SEM image of the fracture surface of a welded joint fabricated using Aluline He5 is shown in Fig. 9a. A ductile fracture was observed in the base material with characteristic dimples. When Aluline He30 was used, the fracture also occurred in the base material, which means WM is stronger than BM. The fracture (Fig. 9b) exhibits the character of a ductile fracture with characteristic dimples on the surface of the fracture. Using He 4.6, the fracture (Fig. 9c) was of the same character as in the previous case. The ductile fracture was also observed when Ar 4.6 was used (Fig. 9d). No pores were observed on the fracture surfaces.

4. Conclusions

The paper investigates the influence of different types of shielding gases on the porosity in the welding of AZ31B magnesium alloy using a disk laser TruDisk 4002. Based on the results, it is possible to state:

– welds created under He 4.6 shielding gas exhibited the smallest width of the weld bead (1.79 mm). Conversely, the weld with the largest width (2.11 mm) was produced if the weld metal was protected by using Ar 4.6 shielding gas,

– the microstructure of the weld metal exhibits dendritic microstructure in all welded joints,

– the lowest volume of porosity in the weld metal was recorded when Ar 4.6 (0.05 mm^3) was used as a shielding gas. Conversely, the highest porosity volume was measured using He 4.6 (0.41 mm^3) as a shielding gas,

– the highest tensile strength of 261 MPa (± 2.4) was recorded if He 4.6 was used. Contrary, the lowest tensile strength of 251 MPa (± 6.8) was recorded when Aluline He30 as a shielding gas was used,

– the smallest measured average microhardness of 71.2 HV0.1 (± 0.6) was recorded under Ar 4.6 shielding gas and, conversely, the highest was detected if the weld metal was protected from the ambient atmosphere by using He 4.6, namely 87.9 HV0.1 (± 0.8),

– in terms of the lowest porosity volume in the weld metal, the following welding parameters appear to be the most suitable: laser power 1.9 kW, welding speed 40 mm s^{-1}, focusing 0 mm, protective atmosphere Ar 4.6 with a shielding gas flow rate of 30 l min^{-1}.

Acknowledgements

This publication was supported by the Operational Programme Research and Innovation for the project: Scientific and Research Centre of Excellence SlovakION for Material and Interdisciplinary Research, code of the project ITMS2014+ : 313011W085 co-financed by the European Regional Development Fund.

References

[1] V. Paradiso, F. Rubino, P. Carlone, G. Palazzo, Magnesium and aluminium alloys dissimilar joining by friction stir welding, Procedia Eng. 183 (2017) 239–244. doi:10.1016/j.proeng.2017.04.028

[2] S. Meco, G. Pardal, S. Ganguly, S. Williams, N. McPherson, Application of laser in seam welding of dissimilar steel to aluminium joints for thick structural components, Opt. Lasers Eng. 67 (2015) 22–30. doi:10.1016/j.optlaseng.2014.10.006

[3] S. Chen, Q. Li, B. Chen, D. Liu, Si diffusion behavior during laser welding-brazing of Al alloy and Ti alloy with Al-12Si filler wire, Trans. of Nonferrous Met. Soc. China 20 (2010) 64–70. doi:10.1016/S1003-6326(09)60098-4

[4] Y. Chen, Q. Ni, M. Ke, Interface characteristic of friction stir welding lap joints of Ti/Al dissimilar alloys, Trans. of Nonferrous Met. Soc. China 22 (2012) 299–304. doi:10.1016/S1003-6326(11)61174-6

[5] W. Oates, Welding Handbook, Materials and Applications, Vol. 3, 8th ed., American Welding Society, Miami, 1996. ISBN: 0871714701

[6] B. Sunil, G. Reddy, A. Mounika, P. Sree, Joining of AZ31 and AZ91 Mg alloys by friction stir welding, J. Magnes. Alloy. 3 (2015) 330–334. doi:10.1016/j.jma.2015.10.002

[7] F. Czerwinski, Welding and joining of magnesium alloys, IntechOpen 2011. doi:10.5772/13947

[8] T. Kramár, Welding of magnesium alloys with concentrated energy sources. Available on http://stc.fs.cvut.cz/pdf13/2640.pdf. (In Slovak)

[9] T. Kramár, Welding of magnesium alloys by selected welding technologies, MTF STU Bratislava, Trnava, 2014. (In Slovak)

[10] Y. Yan, D. Zhang, Ch. Qiu, W. Zhang, Dissimilar friction stir welding between 5052 aluminium alloy and AZ31 magnesium alloy, Trans. of Nonferrous Met. Soc. China 20 (2010) 619–623. doi:10.1016/S1003-6326(10)60550-X

[11] V. Alfieria, F. Caiazzo, V. Sergi, Autogenous laser welding of AA 2024 aluminium alloy: process issues and bead features, Procedia CIRP 33 (2015) 406–411. doi:10.1016/j.procir.2015.06.094

[12] M. Wahba, S. Katayama, Laser welding of magnesium alloys, Trans. of JWRI 41 (2012) 11–23.

[13] I. Hrivňák, D. Hrivňáková, Materiálografia, STU Bratislava, Bratislava, 2011. ISBN 9788022736060. (In Slovak)

[14] D. Dietrich, D. Nickel, M. Krause, T. Lampke, M. Coleman, V. Rande, Formation of intermetallic phases in diffusion-welded joints of aluminium and magnesium alloys, J. Mater. Sci. 47 (2011) 357–364. doi:10.1007/s10853-010-4841-5

[15] M. Vyskoč, M. Sahul, M. Sahul, Effect on shielding gas on the properties of AW 5083 aluminum alloy laser weld joints, J. Mater. Eng. Perform. 27 (2018) 2993–3006. doi:10.1007/s11665-018-3383-x

[16] L. Reis, V. Infante, M. Freitas, F. Duarte, P. Moreira, P. Castro, Fatigue behaviour of aluminium lap joints produced by laser beam and friction stir welding, Procedia Eng. 74 (2014) 293–296. doi:10.1016/j.proeng.2014.06.265

[17] F. Caiazzo, V. Aalfieri, F. Cardaropoli, G. Corrado, V. Sergi, Characterization of disk-laser dissimilar welding of titanium alloy Ti-6Al-4V to aluminium alloy 2024 [C], Proc. SPIE 8603, High-Power Laser Materials Processing: Lasers, Beam Delivery, Diagnostics, and Applications II, (2013). doi:10.1117/12.2004681

[18] S. Chen, L. Li, Y. Chen, J. Dai, J. Huang, Improving interfacial reaction nonhomogeneity during laser welding – brazing aluminium to titanium, Mater. Des. 32 (2011) 4408–4416. doi:10.1016/j.matdes.2011.03.074

[19] K. Kalaiselvan, A. Elango, Effect of butt joint distortion on Ti/Al dissimilar metal using laser beam welding, J. Chem. Pharm. 6 (2015) 65–68. doi:10.5281/zenodo.1338812

[20] J. Blackburn, Ch. Allen, P. Hilton, L. Li, Nd:YAG laser welding of titanium alloys using a directed gas jet, J. Laser Appl. 22 (2010) 71–78. doi:10.2351/1.3455825

[21] J. Sanchez-Amaya, T. Delgado, L. Gonzalez-Rovira, F. Botana, Laser welding of aluminium alloys 5083 and 6082 under conduction regime, Appl. Surf. Sci. (2009) 255: 9512–9521. doi:10.1016/j.apsusc.2009.07.081

[22] F. Sherm, J. Bezold, U. Glatzel, Laser welding of Mg alloy MgAl3Zn1 (AZ31) to Al alloy AlMg3 (AA5754) using ZnAl filler material, Sci. Technol. Weld. Join. 17 (2012) 364–367. doi:10.1179/136217112X13333824902080

[23] A. Batahgy, M. Kutsuna, Laser beam welding of AA 5052, AA 5083, and AA6061 aluminium alloys, Adv. Mater. Sci. Eng. 2009 (2009) 974182. doi:10.1155/2009/974182

[24] P. Kah, J. Martikainen, Influence of shielding gases in the welding of metals, Int. J. Adv. Manuf. Technol. 64 (2013) 1411–1421. doi:10.1007/s00170-012-4111-6

[25] B. Bauer, A. Topic, S. Kralj, Z. Kožuh, Influence of the gas composition on the geometry of laser-welded

joints in duplex stainless steel, Materiali in Tehnologije 45 (2011) 413–419.
[26] M. Glowacki, The effects of the use of different shielding gas mixtures in laser welding of metals, J. Phys. D Appl. Phys. 28 (1995) 2051. doi:10.1088/0022-3727/28/10/009
[27] J. Drábiková, Perspective surface treatment of magnesium alloys. Available on: https://www.vutbr.cz/www_base/zav_prace_soubor_verejne.php?file_id=50795 (In Czech)
[28] T. Kupec, Welding of light alloys by FSW method. [Dissertation Thesis], MTFS STU Bratislava, Trnava (2014). (In Slovak)
[29] Y. Zhao, The effect of shielding gas composition on weld bead geometry during short-circuit GMA welding of Inconel625 alloy. [Master Thesis], TU Delft, Delft (2016).
[30] S. Katayama, Y. Kawahitoa, M. Mizutani, Elucidation of laser welding phenomena and factors affecting weld penetration and welding defects, Phys. Procedia 5 (2010) 9–17. doi:10.1016/j.phpro.2010.08.024
[31] J. Ahn, E. He, L. Chen, J. Dear, C. Davies, The effect of Ar and He shielding gas on fibre laser weld shape and microstructure in AA 2024-T3, J. Manuf. Process. 29 (2017) 62–73. doi:10.1016/j.jmapro.2017.07.011
[32] U. Reisgen, M. Schleser, O. Mokrov, E. Ahmed, Shielding gas influences on laser weldability of tailored blanks of advanced automotive steels, Appl. Surf. Sci. 257 (2010) 1401–1406. doi:10.1016/j.apsusc.2010.08.042
[33] B. Hadzima, Corrosion of Mg-Al-Zn alloys. [Dissertation Thesis], University of Žilina, Žilina (2003). (In Slovak)
[34] M. Sahul, M. Sahul, J. Lokaj, Effect of surface layer on the properties of AZ31 magnesium alloy welded joints, Mater. Today: Proc. 3 (2016) 1150–1155. doi:10.1016/j.matpr.2016.03.015
[35] M. Dhahri, J. Masse, J. Mathieu, J. Barreau, M. Autric, Laser welding of AZ91 and WE 43 magnesium alloys for automotive and aerospace industries, Adv. Eng. Mater. 3 (2001) 504–507. doi:10.1002/1527-2648(200107)3:7<504::AID-ADEM504<3.0.CO;2-3
[36] L. Yu, K. Nakata, J. Liao, Weld porosity in fibre laser weld of thixomolded heat resistant Mg alloys, Sci. Technol. Weld. Join. 14 (2009) 554–558. doi:10.1179/136217109X441209
[37] M.Salleh, M. Ishak, F. Romlay, Effect of fiber laser parameters on laser welded AZ31B magnesium alloys, MATEC Web of conferences 90 (2017) 01032. doi:10.1051/matecconf/20179001032
[38] F. Li, X. Zeng, G. Cao, Investigation of microstructure characteristics of the CVCDEed AZ31 magnesium alloy, Mater. Sci. Eng. A 639 (2015) 395–401. doi:10.1016/j.msea.2015.05.042
[39] M. Haronni, J. Ma, B. Carlson, R. Kovacevic, Two-pass laser welding of AZ31B magnesium alloy, Journal of Materials Processing Technology 216 (2015) 114–122. doi:10.1016%2Fj.jmatprotec.2014.08.028
[40] S. C. Wu, C. Yu, W. H. Zhang, Y. N. Fu, L. Helfen, Porosity induced fatigue damage of laser welded 7075-t6 joints investigated via synchrotron X-ray microtomography, Sci. Technol. Weld. Join. 20 (2015) 11–19. doi:10.1179/1362171814Y.0000000249
[41] D. Chen, X. Zhan, T. Liu, Y. Zhao, N. Qi, L. Sun, Effect of porosity morphology and elements characteristics on mechanical property in T-joints during dual laser-beam bilateral synchronous welding of 2060/2099 Al-Li alloys, Opt. Laser Technol. 140 (2021) 107019. doi:10.1016/j.optlastec.2021.107019
[42] S. C. Wu, C. Yu, P. S. Yu, J. Y. Buffière, L. Helfen, Y. N. Fu, Corner fatigue cracking behavior of hybrid laser AA7020 welds by synchrotron X-ray computed microtomography, Mater. Sci. Eng. A 651 (2016) 604–614. doi:10.1016/j.msea.2015.11.011
[43] K. Fahlström, J. Blackburn, L. Karlsson, L. Svensson, Effect of laser welding parameters on porosity of welds in cast magnesium alloy AM50, MAMS 1 (2018) 25–32. doi:10.32474/MAMS.2018.01.000106
[44] L. Kolařík, M. Kolaříková, P. Vondrouš, Mechanical properties of interface of heterogeneous diffusion welds of titanium and austenitic steel, Key Eng. Mater. 586 (2014) 178–181. doi:10.4028/www.scientific.net/KEM.586.178
[45] Tsung-Yuan Kuo, Yen-Tsun Lin, Effects of shielding gas flow rate and power waveform on Nd:YAG laser welding of A5754-O aluminum alloy, Mater. Trans. 47 (2006) 1365–1373. doi:10.2320/matertrans.47.1365
[46] H. Toda, H. Oogo, K. Horikawa, K. Uesugi, A. Takeuchi, Y. Suzuki, M. Nakazawa, Y. Aoki, M. Kobayashi, The true origin of ductile fracture in aluminum alloys, Metall. Mater. Trans. A 45 (2014) 765–776. doi:10.1007/s11661-013-2013-3
[47] E. Padilla, V. Jakkali, L. Jiang, N. Chawla, Quantifying the effect of porosity on the evolution of deformation and damage in Sn-based solder joints by X-ray microtomography and microstructure-based finite element modeling, Acta Mater. 60 (2016) 4017–4026. doi:10.1016/j.actamat.2012.03.048
[48] K. Takahashi, B. Mehmetli, S. Sato, Influence of shielding gas and laser irradiation conditions on porosity formation in CO_2 laser welding of aluminium alloy, Weld. Int. 12 (1998) 347–353. doi:10.1080/09507119809448498
[49] Ch. Panwisawas, B, Perumal, M. Ward, N. Turner, P. Turner, J. Brooks, H. Basoalto, Keyhole formation and thermal fluid flow-induced porosity during laser fusion welding in titanium alloys: Experimental and modelling, Acta Mater. 126 (2017) 251–263. doi:10.1016/j.actamat.2016.12.062
[50] J. Rudy, E. Rupert, Effects of porosity on mechanical properties of aluminum welds, Welding Journal 49 (1970) 322–336.
[51] S. Wu, X. Yu, R. Zuo, W. Zhang, H. Xie, J. Jiang, Porosity, element loss and strength model on softening behavior of hybrid laser arc welded Al-Zn-Mg-Cu alloy with synchrotron radiation analysis, Welding Journal 92 (2013) 64–71.
[52] S. Sato, J. Matsumoto, N. Okoshi, Effects of porosity on the fatigue strength of 5083 alloy butt welds, Journal of Japan Institute of Light Metals 31 (1976) 398–405. doi:10.2464/jilm.26.398
[53] A. Yadollahi, N. Shamsaei, Additive manufacturing of fatigue resistant materials: Challenges and opportunities, Int. J. Fatigue 98 (2017) 14–31. doi:10.1016/j.ijfatigue.2017.01.001
[54] J. Silva, Laser welding of aluminium rings. Autogenous welding of aluminium alloy AA6082-T651. Online: https://fenix.tecnico.ulisboa.pt/downloadFile/

395142718113/Disk%20Laser%20Welding%20of%20Aluminium%20Rings-Paper.pdf
[55] M. Gao, C. Chen, M. Hu, L. Guo, Z. Wang, X. Zeng, Characteristics of plasma plume in fiber laser welding of aluminum alloy, Appl. Surf. Sci. 326 (2014) 181–186. doi:10.1016/j.apsusc.2014.11.136
[56] J. A. Slotwinski, E. J. Garboczi, K. M. Hebenstreit, Porosity measurements and analysis for metal additive manufacturing process control, J. Res. Natl. Inst. Stand. Technol. 119 (2014) 494–528. doi:10.6028/jres.119.019
[57] K. Heim, F. Bernier, R. Pelletier, L.-P. Lefebvre, High resolution pore size analysis in metallic powders by X-ray tomography, Case Studies in Nondestructive Testing and Evaluation 6 (2016) 45–52. doi:10.1016/j.csndt.2016.09.002
[58] M. Dhahri, J. Masse, J. Mathieu, G. Barreau, M. Autric, Laser weldability of WE43 magnesium alloy for aeronautic industry, Proceedings of the Third Lane 2001: Laser Assisted Net Shape Engineering, 2001.
[59] Z. Wang, M. Gao, H. Tang, X. Zeng, Characterization of AZ31B wrought magnesium alloy joints welded by high power fiber laser, Mater. Charact. 62 (2011) 943–951. doi:10.1016/j.matchar.2011.07.002
[60] H. Zhao, T. Debroy, Pore formation during laser beam welding of die-cast magnesium alloy AM60B – Mechanism and remedy, Welding Journal 80 (2001) 204–210.
[61] V. Stolbov, V. Eltsov, I. Oleinik, V. Matyagin, Effect of the nature of thermal processes on cracking in repair welding components of magnesium alloys, Svarochnoe Proizvodstvo 37 (1990) 29–31. doi:10.1080/09507119109447850
[62] X. Cao, M. Jahazi, J. P. Immarigeon, W.Wallace, A review of laser welding techniques for magnesium alloys, Journal of Materials Processing Technology 171 (2006) 188–204. doi:10.1016/j.jmatprotec.2005.06.068
[63] P. Asadi, K. Kazemi-Choobi, A. Elhami, Welding of Magnesium Alloys, TechOpen 2021. doi:10.5772/47849